Scaling the thrust and deformations of a rotor with flexible blades

Tristan Aurégan, Benjamin Thiria, Sylvain Courrech Du Pont

Scaling the thrust and deformations of a rotor with flexible blades

Tristan Aurégan[1], Benjamin Thiria[1], and Sylvain Courrech du Pont[2]
[1] *Laboratoire de Physique et Mécanique des Milieux Hétérogènes, PMMH UMR 7636 CNRS ESPCI PSL Research University Univ. Paris-Diderot Sorbonne Université, Paris, France. and*
[2] *Laboratoire Matière et Systèmes Complexes, UMR CNRS 7057, Université de Paris Bt. Condorcet, Paris, France.*
(Dated: April 17, 2023)

Adding flexibility to rotating structures has been shown to improve their efficiency and reliability as well as their compliance to external flow perturbations. Here, we experimentally investigate the problem of a propulsive rotor submerged in water with flexible blades in both spanwise and chordwise directions. When we rotate the propeller and set an incoming flow, the blades bend and twist. We report measurements of forces and associated blade deformations. We show that moderate deformation affect the thrust produced by the rotor within a few percent while strong deformation completely inhibit thrust production. We show that the bending angle of the blade can be predicted thanks to a modified Cauchy number taking into account the angle of attack of the blade, in the limit of small deformations. Finally we show that there exist a single curve linking the thrust produced by the rotor to the bending deformation.

I. INTRODUCTION

Rotors are ubiquitous in man-made propulsion systems or energy harvesting devices. Traditionally these rotors are made stiff to avoid potential destructive deformations : wind turbines have to be designed to avoid blades bending and preventing them from colliding with the mast in high winds. The use of composite materials in many applications makes these deformations unavoidable. Thus, flexibility has to be taken into account in the design process [Hussain et al. 2021, Young 2008]. For helicopters or micro air vehicles highly flexible bladed rotors naturally occur as well : for safety in small drones [Lv et al. 2015, Nguyen et al. 2020] or to build retractable systems such as Sicard and Sirohi [2016] where the blades can be rolled into the hub. Understanding the fluid forcing on the blades of these systems is fundamental to meet thrust or efficiency requirements.
In general, the effect of flexibility on objects subjected to flows is to improve their compliance to variations of external conditions. The behavior of plants in flows has been widely studied [de Langre 2008, Gosselin and de Langre 2011, Schouveiler and Boudaoud 2006] and their flexibility allows them to reduce their drag and thus survive extreme events. In the case of rotating structures, we know that flexible deformations can be beneficial for performance. Indeed, Motley et al. [2009] have shown that, using the anisotropic properties of composite materials, the off-design efficiency of marine propellers can be improved by tuning the flexibility. There is a fundamental relation between the deformation of a rotating structure and the distribution of forces on a blade. Subtle changes in twist can transform the response of a rotor to the same conditions. Cognet et al. [2017, 2020] have shown that given a wind turbine design and a wind distribution, it is possible to find elastic properties which increase the performance of the turbine by widening its operating range. Recently Durán Venegas et al. [2019] have proposed a mathematical description of a propeller where the fluid forcing as well as the centrifugal force bend the blades while in rotation.
Here we experimentally study the canonical problem of a propeller with highly flexible blades where the main driver of deformation is the flow itself, which can be either imposed externally or produced by the rotation. The goal of this work is to get a better understanding of the fluid forcing on the blades and its effect on the propeller thrust. To do so, we need a system where the fluid force is always much more important than the centrifugal force : this is accomplished by using blades made out of plastic sheets rotating in water.
Eldemerdash and Leweke [2021a] have recently studied a very similar system of a rotor made out of slender, flexible plastic blades in water. They measured the flow field around the blades as well as the deformations and shown that important bending can be observed (greater than 90° in some cases) in forward motion as well as large amplitude oscillations in backwards motion. In their study, the thrust is estimated for some parameters using the flow field but no direct measurement was made. In the present paper, we directly measure the thrust produced by such a propeller and how it is modified by the blades deformation. We are interested in the propulsive performance of such a propeller in water. Thus, there are two key differences between this work and the work of Eldemerdash and Leweke [2021a] : we only study forward motion and we use a wider range of pitch angles. These changes correspond to the parameters typically found in boat or plane propellers moving forward instead of helicopters or small drones hovering. We use the mathematical description of the system based on the work of Durán Venegas et al. [2019] to show how the thrust of a flexible rotor is modified by the addition of flexibility. Then, we can understand the small deformations through the modification of the classical Cauchy number. Finally, we link the bending of the blades with the thrust produced by the rotor and show that it is sufficient to know the deformation of the propeller to predict the produced thrust.

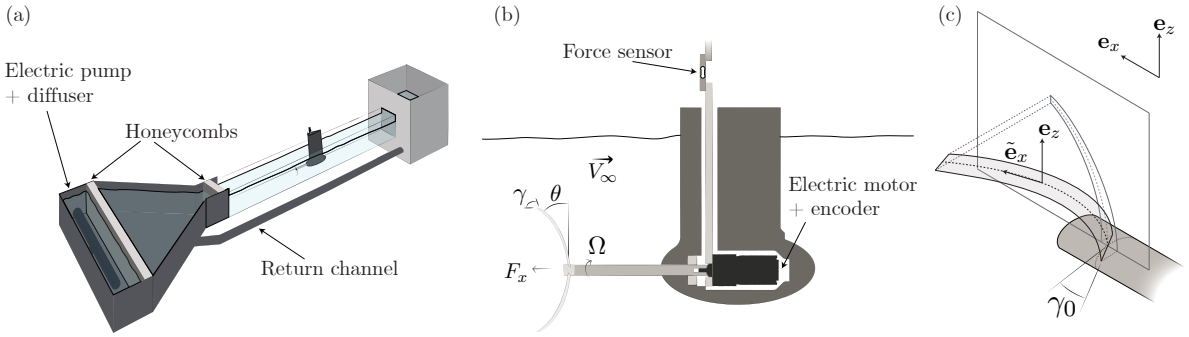

FIG. 1. Sketch of the experimental setup. (a) Water channel (proportions respected), (b) cut of the hull and rotor, (c) sketch of the out of plane bending of the blades. The vertical grey plane corresponds to the image of the blade as seen by a camera infinitely far away.

II. EXPERIMENTAL SETUP

We perform experiments in a free surface water channel in a closed loop with a 0.2 m by 0.2 m section. A variable speed pump generates flows from 0.05 to 0.25 m/s in the channel. Using a PIV system we measure the relationship between the pump's rotation speed and the mean velocity and consider it unchanged by the addition of the rotor. The turbulence intensity is below 5% throughout the full range of velocities thanks to a converging section and a series of honeycombs (see Fig. 1 (a)). We mount the flexible blades on a rotating shaft powered by an electric motor able to achieve speeds up to 10 rotations per second and use a Hall effect sensor to precisely measure the rotation speed of the shaft. The electrical components : the sensors, the motor and the wires are inside a protecting hull to avoid corrosion. The hull is 3D printed, has a NACA profile to achieve low drag and is located downstream of the rotor to minimize disturbances (See Fig. 1 (b)). We measure the resultant force along the streamwise direction (sum of the thrust produced by the rotor and hull drag) using a force sensor. In the following, we always remove the hull drag by subtracting the force measured without blades at any given flow speed (the hull drag is about 10^{-2} N, 10 times smaller than the typical thrust.

We use three types of blades in the experiments. All are rectangular with an external radius $R = 46$ mm, an internal radius $R_{\text{hub}} = 4$ mm and a chord $c = 6$ mm but different thicknesses and materials. The rigid blades used for reference are made of thin aluminium sheets and the two sets of flexible blades are cut out of mylar sheets with two different thicknesses. We measure their Young modulus E via a traction measurement using an Instron force sensor. The physical parameters of the blades are displayed on table I. We clamp the blades to the rotating shaft using 3D printed parts with tilted slits to set the pitch angle relative to the plane of rotation. We carry out experiments with pitch values of $5, 10, 20$ and 30 degrees. The blades are attached to a shaft with a diameter of 4 mm and a length of 75 mm in front of the hull.

Blade type	Thickness e (μm)	Young's Modulus (GPa)	Bending modulus EI (N.m^2)	Torsion modulus GJ (N.m^2)
Rigid (aluminium)	460 ± 10	Considered infinite	Considered infinite	Considered infinite
F1 (mylar)	330 ± 10	3.9 ± 0.2	$(6.94 \pm 0.81)\ 10^{-5}$	$(9.69 \pm 1.13)\ 10^{-5}$
F2 (mylar)	110 ± 10	4.0 ± 0.5	$(3.67 \pm 0.64)\ 10^{-6}$	$(5.25 \pm 0.91)\ 10^{-6}$

TABLE I. Relevant physical constants of the blades used in the experiments

We use a high speed camera to directly measure the deflection of the blades under load : it is synchronized with the rotation of the blades using the Hall effect sensor. A frame is shot each time the blades are perpendicular to the line of sight of the camera (see Fig. 2). We track the flexion angle by computing the position of the centerline of a blade and correct for the out of plane bending of the blades. The torsion angle can also be estimated by measuring the thickness of a section of the blade. However this method has low precision and the torsion angles are small so that conclusive results cannot always be obtained.

We show a sketch of the required correction to obtain the bending angle in Fig. 1 (c). In general, the blade bends in 3 dimensions. However Eldemerdash and Leweke [2021a] showed that the twist of the blade is small (of the order of a few degrees compared to the pitch of the blades which is of tens of degrees). As a consequence, we can consider that the blade centerline is in a plane. This means that the vector $\mathbf{d}_1(s)$ defined locally in Fig. 3 is actually of constant direction. The plane containing the centerline is obtained by rotating the vertical plane of Fig. 1 (c) around the vector $\mathbf{e}_z$ by the pitch angle of the blade γ_0. The camera we used to measure the bending angle is placed sufficiently

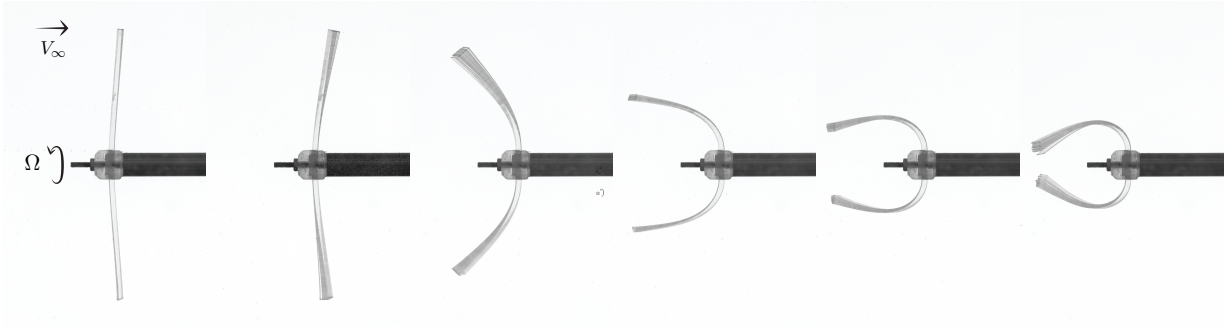

FIG. 2. Typical deformation of the blades when the rotational velocity is increased (superposition of approximately 30 phase synchronous frames). Blades F2 with 20 deg incident angle subjected to 0.08 m/s flow, with increasing rotational velocity from 0 to 30 rad/s

far away (about 2 m) to be considered at infinity and thus captures the shape of the blade as projected onto the vertical plane. The distances measured along the x direction are thus underestimated if not corrected. In order to get the actual shape of the blade in the plane of bending we correct the distances by a factor $1/\cos\gamma_0$.

For each set of parameters we capture at least 30 images, extract data separately and use the mean of the results as the flexion angle. Similarly, we average values of rotational velocity and force measurements over 20 s, after a 10 s settling period when the electric motor is turned on.

Throughout the study, we use lift and drag coefficients based on high Reynolds number theory. The relevant Reynolds number in our experiments is based on the chord length and the local relative velocity seen by a blade section :

$$Re(r) = \frac{c\sqrt{V_\infty^2 + (r\Omega)^2}}{\nu} \tag{1}$$

where ν is the kinematic viscosity of water and r is the distance from the axis of rotation. At mid span, this gives a range $Re \in [750, 5000]$ and while being on the lower end this allows us to use the airfoil theory (See Lissaman [1983], Mateescu and Abdo [2010] for an analysis of low Reynolds lifting devices).

III. MATHEMATICAL DESCRIPTION

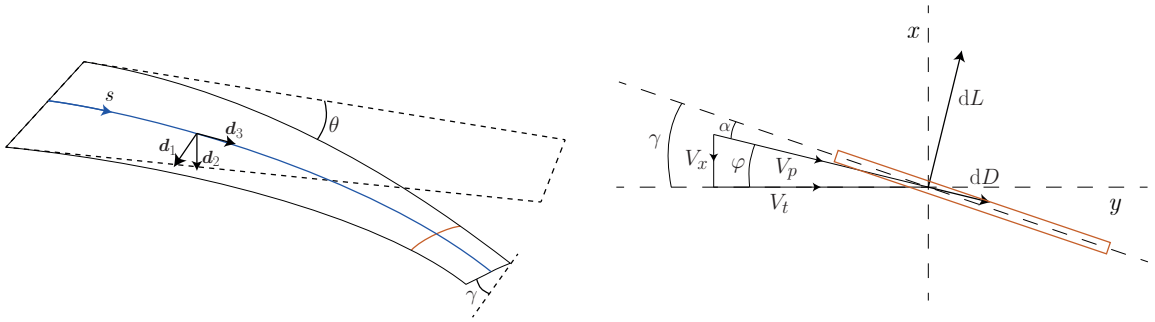

FIG. 3. Left, axes and angles definition on the blade. Right, angles and definitions on a cut (orange line) of the blade

We obtain the equations describing the deformation of the blades in a similar fashion as in Durán Venegas et al. [2019] but with a few key differences. First the blades are submerged in water, modifying the balance of the forces acting on the blades. We also use important pitch angles (up to 30 degrees) and so small angles limits used in this article are not valid here. Finally our blade shape is rectangular and flat, simplifying the constitutive relation.

Using Kirchhoff relations for a steady state in the local frame $(\boldsymbol{d}_1, \boldsymbol{d}_2, \boldsymbol{d}_3)$ described in Fig. 3, we have :

$$\begin{aligned} \frac{\partial \boldsymbol{T}}{\partial s} + \boldsymbol{f} &= \boldsymbol{0}, \\ \frac{\partial \boldsymbol{M}}{\partial s} + \boldsymbol{d}_3 \times \boldsymbol{T} + \boldsymbol{m} &= \boldsymbol{0}, \end{aligned} \tag{2}$$

where $\boldsymbol{f}$ and $\boldsymbol{m}$ are the external forces and moments per unit of length respectively, while $\boldsymbol{T}$ and $\boldsymbol{M}$ are the internal elastic forces and moments. The vector $\boldsymbol{d}_3$ is tangent to the blade centerline (defined along the centers of mass of each section). We assume that our rectangular blades behave like inextensible ribbons and thus the constitutive law is :

$$\boldsymbol{M} = EI\kappa_1 \boldsymbol{d}_1 + \frac{EJ}{2\,(1+\nu)}\tau \boldsymbol{d}_3, \tag{3}$$

where ν is the Poisson ratio, E is the Young modulus, I is the second moment of area in the $\boldsymbol{d}_1$ direction and J the torsion modulus of the blade. The complete elastic energy for inextensible ribbons contains non quadratic and coupled terms between the bending and torsion curvatures (see Audoly and Neukirch [2021]). However in the present study, given that our blades are slender and thin and that twisting curvature remains small the simpler relation (3) here remains valid.

The external forces acting on a blade are the hydrodynamic forces and the centrifugal force. We separate the fluid force in lift and drag coefficients acting on each section of the blade normal to its span (see orange cut in Fig. 3). In this frame, the force normal to the surface of the blade reads :

$$F_{\text{hydro}} = \frac{1}{2}\rho V_p^2 c \left(C_L(\alpha)\cos\alpha - C_D(\alpha)\sin\alpha\right), \tag{4}$$

where ρ is the fluid density, V_p is the local apparent velocity (see Fig 3), c the chord of the blade, C_L and C_D are respectively the profile lift and drag coefficients and α is the local angle of attack. Writing the hydrodynamic force as such, we neglect any contribution of radial flow along the span of the blades. As long as the bending is small to moderate, this spanwise description of rotating systems has been shown to be a good approximation (see for instance Cognet et al. [2020], Durán Venegas et al. [2019]).

The centrifugal force tends to align the blade with the plane of rotation. It has in general a component in the $\boldsymbol{d}_2$ and $\boldsymbol{d}_3$ directions, however external forces in the $\boldsymbol{d}_3$ direction do not contribute to the bending and twisting as can be seen in equation (2). The centrifugal force per unit span projected in the $\boldsymbol{d}_2$ direction reads :

$$F_{\text{centrifuge}} = A_b \rho_b \tilde{r} \Omega^2 \boldsymbol{e}_r \cdot \boldsymbol{d}_2, \tag{5}$$

where A_b is the cross-sectional area of the blade, ρ_b its density and Ω the rotation speed. The distance to the rotation axis is denoted as $\tilde{r}$, which in the limit of small twist equals :

$$\tilde{r}^2 = \left(r_{\min} + \int_{r_{\min}}^{R} \cos\theta \mathrm{d}s\right)^2 + \left(\sin\gamma_0 \int_{r_{\min}}^{R} \sin\theta \mathrm{d}s\right)^2. \tag{6}$$

The vector $\boldsymbol{e}_r$ is the unit vector aligned with the direction of the centrifugal force : it is pointed radially with no component in the vertical direction. The expression of the projection $\boldsymbol{e}_r \cdot \boldsymbol{d}_2$ can be computed analytically, but the complete formula is not necessary for the discussion here since the centrifugal will be negligible as discussed in the following. Combining together the Kirchhoff equations (2), the constitutive law (3) and the external forces, the equation describing the bending of the blade during the rotation reads :

$$EI\frac{\partial^3 \theta}{\partial s^3} = \frac{1}{2}\rho V_p^2 c \left(C_L(\alpha)\cos\alpha - C_D(\alpha)\sin\alpha\right) - A_b \rho_b \tilde{r} \Omega^2 \boldsymbol{e}_r \cdot \boldsymbol{d}_2. \tag{7}$$

The hydrodynamic center of a typical airfoil is located around 1/4 of the chord and since the blades have an homogeneous and rectangular profile, their center of mass is located at mid chord. Thus, the blades tend to twist and increase their pitch angle when they generate lift due to the hydrodynamic moment. The centrifugal force tends to resist this twist and brings the blade towards the plane of rotation. Similarly, to the bending equation, we obtain for the torsion :

$$\frac{EJ}{2(1+\nu)}\frac{\partial^2 \gamma}{\partial s^2} = -\frac{1}{2}\rho_b c^2 V_p^2 \left(\left(C_L(\alpha)\cos\alpha + C_D(\alpha)\sin\alpha\right)\bar{\delta}_{cm}^{ac}\right) + \frac{\rho e c^3 \Omega^2}{12}\sin 2\gamma \cos\theta, \tag{8}$$

where $\bar{\delta}^{ac}_{cm}$ is the algebraic distance between the aerodynamic center and the center of mass (equal to $1/4c$ in general but which can slightly deviate from this value depending on the angle of attack [Li et al. 2022]). In our problem the typical length scale is R and the typical speed is $R\Omega$. A common parameter for rotating systems thus appears : the reduced velocity or tip speed ratio $\lambda = R\Omega/V_\infty$. We use these quantities to make the equations of the deformation dimensionless and two Cauchy (or elastohydrodynamical) numbers appear : for the bending of the blades and for the twist respectively. They compare the intensity of the hydrodynamic forces to the elastic moduli and read :

$$C_Y^B = \frac{\rho S_b (R\Omega)^2 R^2}{2EI}, \quad C_Y^T = \frac{\rho S_b (R\Omega)^2 Rc(1+\nu)}{EJ}. \tag{9}$$

The system of elastic equations in dimensionless form reads :

$$\frac{1}{C_Y^B}\frac{\partial^3 \theta}{\partial s^3} = U_p^2 \left(C_L(\alpha)\cos\alpha + C_D(\alpha)\sin\alpha\right) - 2d\frac{A_b}{S_b}\frac{\tilde{r}}{R}\boldsymbol{e}_r \cdot \boldsymbol{d}_2, \tag{10}$$

$$\frac{1}{C_Y^T}\frac{\partial^2 \gamma}{\partial s^2} = -U_p^2 \left[\left(C_L(\alpha)\cos\alpha + C_D(\alpha)\sin\alpha\right)\delta^{ac}_{cm} + C_{m_0}\right] + \frac{1}{12}\frac{A_b}{R^2}\sin 2\gamma \cos\theta, \tag{11}$$

where $U_p = V_p/R\Omega$, $\delta^{ac}_{cm} = \bar{\delta}^{ac}_{cm}/c$, $d = \rho_b/\rho$ is the density of the blade, and S_b is the planar surface of a single blade. Note that going from Eq. (7) to (10) the curvilinear abscissa has been transformed from a dimensional variable to its dimensionless counterpart (also referred to as s for convenience) by dividing by R. This lets us to compare the order of magnitude of the different terms :

$$2d\frac{A_b}{S_b} \approx 10^{-2} \quad \text{and} \quad \frac{A_b}{12R^2} \approx 10^{-5} \quad \text{while} \quad U_p \approx \sqrt{1+\frac{1}{\lambda^2}} \approx 1. \tag{12}$$

The centrifugal force and moment are orders of magnitude smaller than the hydrodynamics contribution but for very large deformation (i.e. large Cauchy numbers). In the following we neglect the centrifugal force and focus on the coupling between the elasticity and the fluid loading.

IV. RESULTS AND DISCUSSION

We perform the experiments at a fixed flow speed V_∞ (0.05 to 0.15 m/s) and pitch angle γ_0, and increasing the angular velocity from 0 to 35 rad/s. Figure 4 shows the results of experiments for $V_\infty = 0.15$ m/s and $\gamma_0 = 20$ deg. We plot two quantities of interest : the thrust produced by the rotor and the tip bending angle $\theta_M = \theta(s = R)$. We can see that both flexible blades exhibit significant bending deformations at large tip speed ratios. The F1 blades have similar thrust than their rigid counterpart while the F2 blades almost completely fold along this axis of rotation ($\theta_M > \pi/2$, see Fig. 2) thus generating almost zero thrust. Note that at zero angular velocity, the upstream flow on its own is not strong enough to bend the F1 blades but does slightly bend backwards the F2 blades. These most flexible blades also sometimes exhibit different behaviors for the two blades with the same external conditions (see Fig 4 (bottom), red markers at 10 rad/s $< \Omega <$ 15 rad/s). We believe this is most likely due to small experimental deviations on the exact clamp angle of the blades. This small pitch difference becomes significant when the loading on the blades varies rapidly with the angle of attack (i.e. when the angle of attack is close to zero). This is why we see the different behavior only close to the angular velocity where sign of the bending changes (Eldemerdash and Leweke [2021a] have also noticed a similar behavior in their experiements).
To compare in more details the thrust produced by different rotors, we introduce the normalized thrust coefficient C_T defined from axial thrust F_x as :

$$C_T = \frac{F_x}{\frac{1}{2}\rho S_b (R\Omega)^2}. \tag{13}$$

The thrust coefficient of the three rotors are shown in Fig. 5 for all pitch angles tested and a fluid velocity of 0.05 m/s. Considering the performance of the reference rigid rotor (blue markers) : the thrust is always negative for the lowest pitch angle of 5 degrees, meaning that the rotor actually works as a brake. For higher pitch angles, the thrust is negative at low tip speed ratio and reaches positive values at higher values of λ. The range of positive thrust can first be estimated by a geometrical argument : the angle of attack at the tip of the blade must be positive, giving the relation

$$\lambda > \frac{1}{\tan\gamma_0}. \tag{14}$$

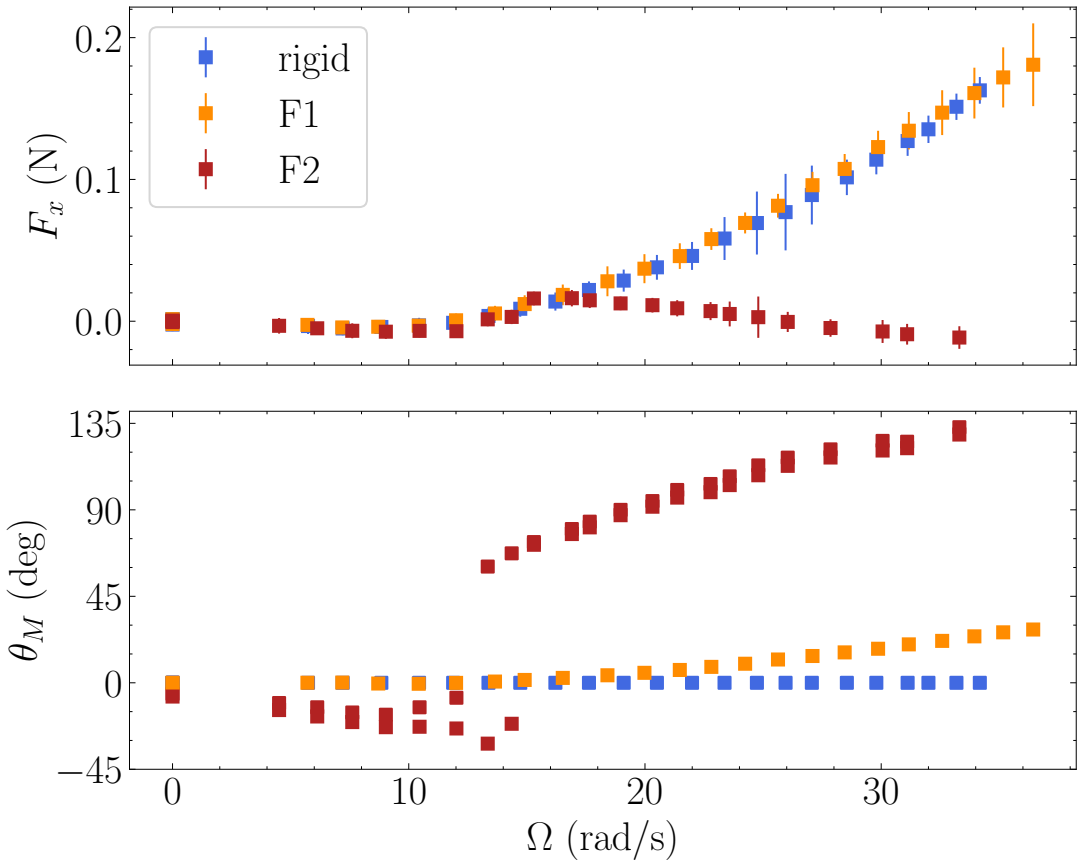

FIG. 4. Thrust force generated by the rotor (top) and deflection of the blade's tip (bottom) as a function of the rotation rate. Blue points correspond to the rigid blades, orange to the lightly flexible ones (F1 in table I) and red to the very flexible ones (F2 in table I). The error bars indicate the standard deviation of the measurement. The standard deviation of the tip bending angle is smaller than the marker size. All curves have the following parameters : $V_\infty = 0.15$ m/s, $\gamma_0 = 20$ deg. The F2 rotor exhibit two sets of points for the bending angle θ_M at a single angular velocity Ω because the two different blades comprising the rotor bend differently.

This threshold is underestimated since it detects a positive angle only at the tip of the blade. Some parts of the blade closer to the hub might still produce negative thrust since the angle of attack grows along the span of the blade.

The most flexible blades start at very low tip speed ratios with a performance similar to the rigid ones but very quickly significantly deviate from the reference behavior. At high tip speed ratios, whichever the pitch angle, F2 blades (red markers) do not produce any thrust. For the intermediate blades F1 (orange markers) the thrust coefficient only decreases at very high tip speed ratios and for high pitch angles Otherwise we observe a similar performance for F1 blades and the rigid ones with a slight increase in thrust production for intermediate tip speed ratios.

Cognet et al. [2017] have found that flexibility can lead to an increase in performance of wind turbines. It should be noted that our system is not suitable for this type of application. Indeed, here the centrifugal force is negligible and our blades twist around their centerline instead of their leading edge. These two differences mean that the flexibility can only increase the angle of attack of the blade. It is the opposite in Cognet et al. [2017] where the aerodynamic loading and centrifugal force act in opposite directions and thus can be tuned to passively adapt to a change in external conditions. In our system, twisting could be used to improve the efficiency of the blade only if the pitch is too small for the operating conditions and if the bending is limited.

We now consider the effect of the fluid loading on the rotor shape to link it with the observations on the thrust production above. This deformation is characterized by two functions along the blade : the bending angle $\theta(s)$ and the twist angle $\gamma(s)$. The twist is small in experiments (described in more extensive details in Eldemerdash and Leweke [2021a]) and so we will focus on the bending angle. Figure 6 shows the tip bending angle for flexible blades as a function of the bending Cauchy number. As expected, for C_Y^B lower than one (corresponding to slow angular velocities and stiffer blades), deformations are small. For larger angular velocities (larger C_Y^B), flexible blades exhibit widely different behavior depending on the pitch angle : the bending deformation is a fast growing function of the

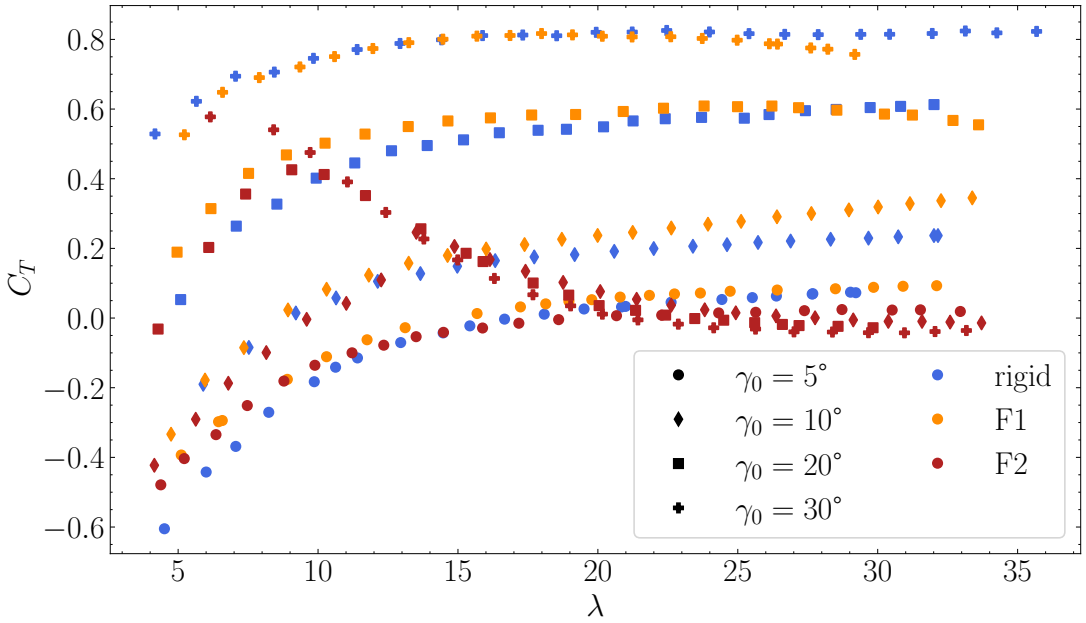

FIG. 5. Thrust coefficient as a function of the tip speed ratio for all rotors tested at $V_\infty = 0.05$ m/s. Markers indicate the pitch angle at the root of the blades (circle : 5 deg, diamond : 10 deg, square : 20 deg, plus : 30 deg), color indicates the blade type (blue : rigid blades, orange : F1 flexible blades, red : F2 flexible blades).

pitch angle. The blades with pitch $\gamma_0 = 5$ deg. bend backwards in almost every flow condition (also for larger incoming velocity V_∞, not shown in Fig. 6) : this corresponds to a negative thrust produced by the rotor and a negative local lift on the blades causing it to bend downstream. The blades with $\gamma_0 = 10$ deg. however, bend backwards for small angular velocities but quickly jump to positive bending when the threshold between positive and negative thrust is reached (red diamonds, around $C_Y^B = 30$). It corresponds to the same threshold as the one described above for the thrust, which can be approximated by (14). Similar behaviors can be observed with the F1 blades but with a much smaller amplitude. Changing the pitch angle by a few degrees can modify the resulting deformation from slightly backwards to 15 or 20 degrees forwards.

In the following, we aim at understanding the different bending angle behavior depending on the pitch angle using a scaling law and geometric arguments. Because it is constructed using small deformation assumptions this scaling law will *a priori* be applicable only to small or moderate Cauchy numbers but gives insight into which physical phenomena drive the deformations. Deriving a scaling law for θ_M from equation (10) we obtain :

$$\theta_M \sim C_Y^B \left(1 + \frac{1}{\lambda^2}\right) \left(C_L(\alpha_M)\cos(\alpha_M) + C_D(\alpha_M)\sin(\alpha_M)\right) \tag{15}$$

We approximate the local apparent velocity at the tip by the combination of both the incoming flow velocity and angular motion (thus neglecting any induced velocity from the rotation). As a first approximation, using the zero twist limit, the angle of attack at the tip becomes

$$\alpha_M \approx \gamma_0 - \arctan\frac{1}{\lambda}. \tag{16}$$

In typical operating conditions, the tip angle of attack is small so that (i) the contribution from the lift coefficient is greater than the one from the drag coefficient and thus we can neglect the second term in (15). And (ii) we can use the linear aerodynamics limit where the lift coefficient is proportional to the angle of attack and get :

$$\theta_M \sim C_Y^B \left(1 + \frac{1}{\lambda^2}\right) \left(\gamma_0 - \arctan\frac{1}{\lambda}\right) \tag{17}$$

In this scaling law, the Cauchy number is rescaled by the lift coefficient of the equivalent rigid rotor. This is similar to the strategy employed in Gosselin et al. [2010], Gosselin and de Langre [2011] where the authors compare the reconfiguration of very different systems by rescaling the Cauchy number by the rigid drag coefficient of the studied system.

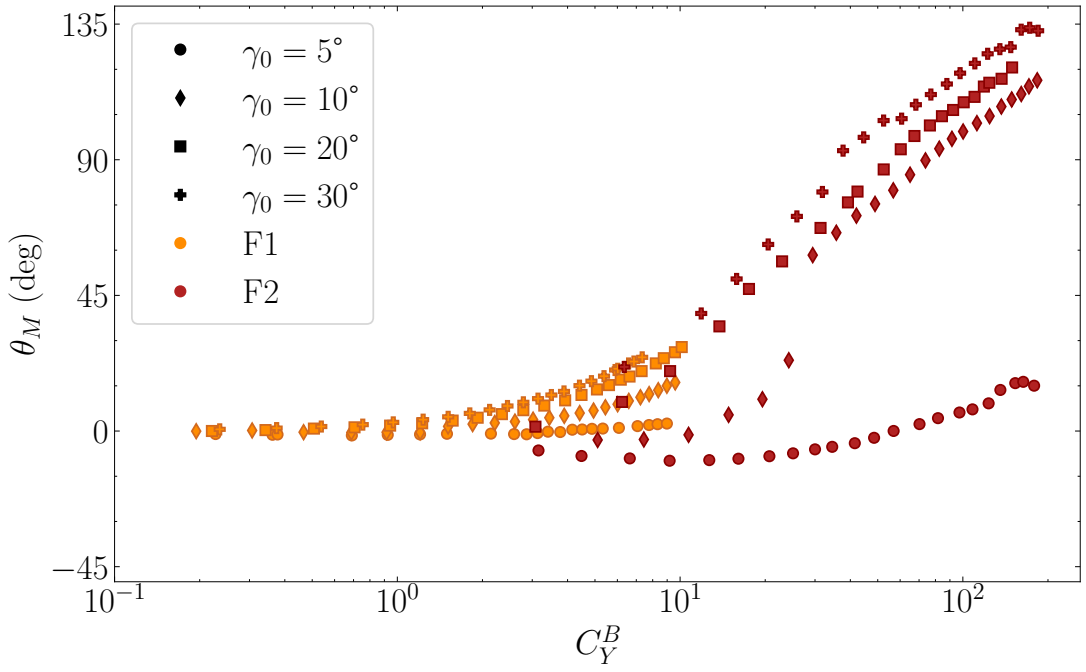

FIG. 6. Tip bending angle θ_M as a function of the bending Cauchy number C_Y^B (9) for all flexible blades tested at $V_\infty = 0.05$ m/s in log scale. Markers indicate the pitch angle at the root of the blades (circle : 5 deg, diamond : 10 deg, square : 20 deg, plus : 30 deg), color indicates the blade type (orange : F1 flexible blades, red : F2 flexible blades).

This scaling law is plotted in Fig. 7 for the F1 blades which experience moderate deformations. the rescaling lest the data reasonably collapse onto a single line of slope approximately 0.15 rad. This indicates that the problem of knowing *a priori* the deformed shape of the blades can be simplified to a geometrical problem that consists in comparing two angles : the pitch angle γ_0 and the apparent flow angle at the tip $\arctan 1/\lambda$. In particular, the positive or negative bending of the blades is completely set by the sign of the modified Cauchy number. This result can be linked to an observation made by Eldemerdash and Leweke [2021b] : when the bending angle of the blade changes sign it is associated with a change of sign of the vorticity created at the blade tip. This sign is itself directly correlated to the local angle of attack at the tip. This shows that our approximation of the angle of attack (16) is valid near zero.
Still, the dispersion of the points is fairly important, in particular at large bending angles. This is due to the multiple hypothesis made to obtain this law. The most important ones being the assumptions that there is no twist between the root and the tip of the blade (while the twist is small, since the lift coefficient is proportional to the angle of attack any deviation has a strong influence on the bending of the blades) and using only the tip values instead of the integral over the blades. The twist is visible in the experiments but difficult to measure accurately. We can still see from Eq. (11) that the forcing term for the twist is proportional to the forcing term for the bending angle. This means that large deformations in the bending direction corresponds to important twist as well. This also explains why the linear dependency of the bending angle with respect to the modified Cauchy number shown in Fig. 7 for the F1 blades does not hold anymore for the large deformations experienced by the F2 blades.
In order to incorporate the effects of a small but non zero twist into a predictive scaling law, Eq. (16) has to be modified to include twist effects (e.g. a contribution proportional to the twisting Cauchy number). One other possible improvement to better estimate the effective angle of attack on the blades would be to couple the bending and twisting equations to a rotor model that computes the flow around the propeller (e.g. the classical Blade Element Momentum Theory [Glauert 1983] or a more complete wake model like in Durán Venegas et al. [2019]).
However, in the following we derive a scaling law that allows to collapse the tip bending angle onto a master curve without explicitely taking the twist into account. In order to do so, we rewrite Eq. (10) using the theoretical thrust and torque coefficients :

$$\begin{aligned} C_T &= \frac{N_b}{1/2\rho S_b (R\Omega)^2} \int_{R_{hub}}^{R} \frac{1}{2}\rho c V_p^2 \left(C_L(\alpha)\cos\varphi - C_D(\alpha)\sin\varphi\right)\cos\theta \mathrm{d}r, \\ C_Q &= \frac{N_b}{1/2\rho S_b R (R\Omega)^2} \int_{R_{hub}}^{R} \frac{1}{2}\rho c V_p^2 \left(C_L(\alpha)\sin\varphi + C_D(\alpha)\cos\varphi\right)\tilde{r}\mathrm{d}r. \end{aligned} \tag{18}$$

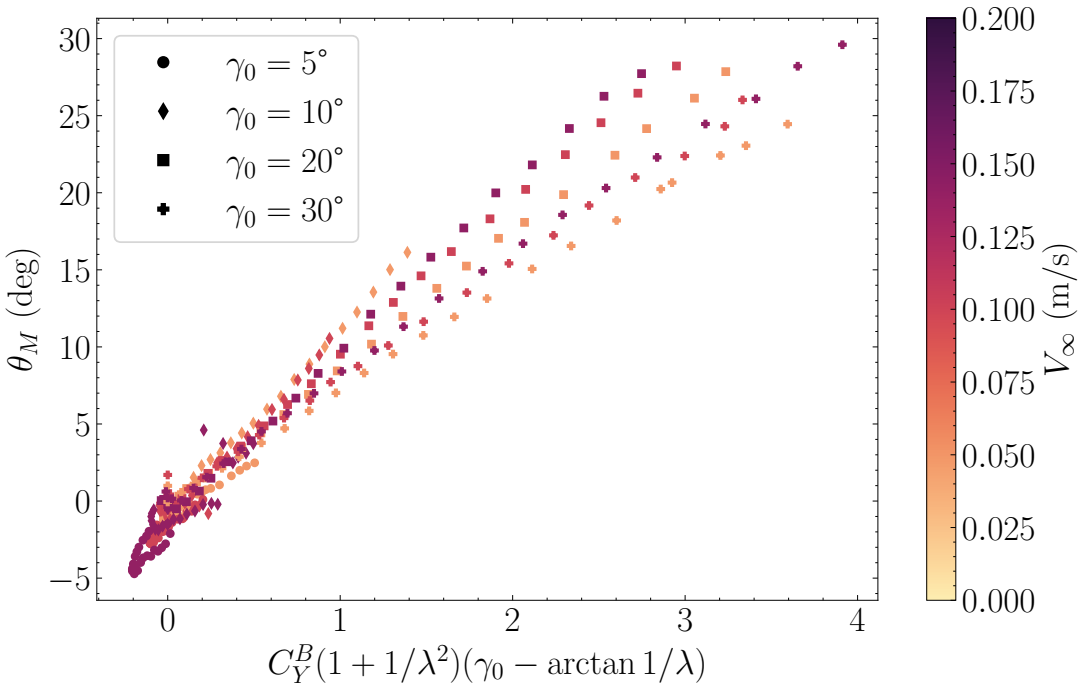

FIG. 7. Tip bending angle θ_M as a function of a modified Cauchy number scaled by the tip velocity and angle of attack for the F1 blade

where N_b is the number of blades. Using the values at the tip of the blade (subscript M), the scaling of these two coefficients is :

$$\begin{aligned} C_T &\sim N_b U_p^2 \left(C_L(\alpha_M)\cos\varphi_M - C_D(\alpha_M)\sin\varphi_M\right)\cos\theta_M, \\ C_Q &\sim N_b U_p^2 \left(C_L(\alpha_M)\sin\varphi_M + C_D(\alpha_M)\cos\varphi_M\right)\cos\theta_M. \end{aligned} \tag{19}$$

By replacing α by $\gamma - \varphi$ in the sines and cosines of Eq. (10) and neglecting the centrifugal force we get :

$$\frac{1}{C_Y^B}\frac{\partial^3\theta}{\partial s^3} = U_p^2\left[\cos\gamma\left(C_L(\alpha)\cos\varphi - C_D(\alpha)\sin\varphi\right) + \sin\gamma\left(C_L(\alpha)\sin\varphi + C_D(\alpha)\cos\varphi\right)\right]. \tag{20}$$

Rewriting this equation as a scaling law, using the values at the tip and using the fact that the twist is small compared to the pitch angle, we can substitute the lift and drag coefficients by the thrust and torque :

$$\theta_M \sim \frac{C_Y^B}{N_b\cos\theta_M}\left(C_T\cos\gamma_0 + C_Q\sin\gamma_0\right), \tag{21}$$

We are interested in describing the small to moderate deformations of the rotor which means that we can make two simplifications to this relationship. First the cosine on the right hand side can be linearized to 1 in the small angle limit. Next, in normal propeller operating conditions, the thrust coefficient produced by the rotor roughly 10 times larger than the torque coefficient (see for instance Young [2008] for typical performance curve of a marine propeller). The previous relationship can thus be simplified to :

$$\theta_M \sim \frac{C_Y^B C_T\cos\gamma_0}{N_b}, \tag{22}$$

where we measure all the terms experimentally. This scaling law gives, for small deformations, a linear relationship between θ_M and integrated, measurable parameters of the rotor.
This new scaling relationship is plotted in Fig. 8. For the F2 blades, in the cases where the two blades exhibit different behaviors we use the mean bending angle between the two blades since the thrust produced by the rotor is the result of the integration of the lift on both blades. We can see that indeed all the data for small bending angles (positive or negative) collapse on the same line. This region of linear relationship strikingly extends from -30 degrees to 40

degrees of bending, way further than the predictive scaling law (17). In this previous relationship we neglected any feedback from the deformation onto the loading itself as well as any twist along the blades. The collapse of all data on this curve but not on Fig. 7 shows that these assumptions are not true for moderate bending angles. However the fact that our new scaling (22) works demonstrates that these non linearities are all taken into account in the thrust coefficient (or are small enough to not be visible).

We can then note that beyond the limits of the linearity of the scaling law, all the data still collapse on a single curve. This curve is not linear and features more dispersion than the linear part. Still it means that for all external conditions tested, the scaling law makes a link between the thrust produced by the rotor and the bending angle. For a given propeller geometry, for all (positive) pitch angle values, this indicates that experimentally measuring one or the other is equivalent. For instance measuring only the bending deformation gives without ambiguity the thrust produced by the rotor if its bending Cauchy number and pitch angle are known.

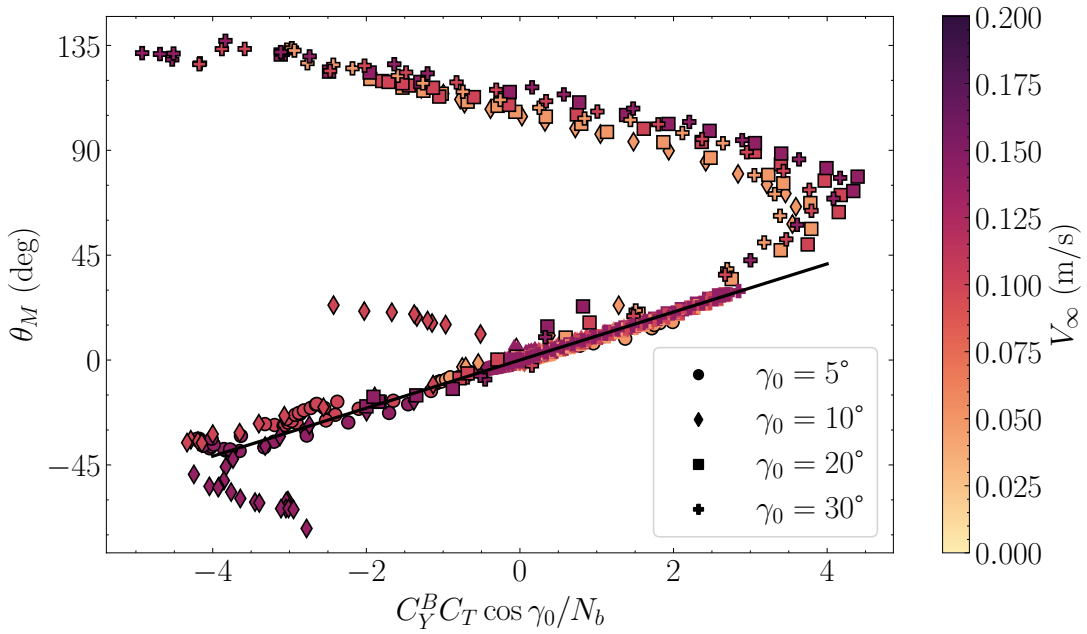

FIG. 8. Flexion angle as a function of the modified Cauchy number scaled by the thrust coefficient. Colors indicate the flow velocity, markers show the blade pitch angle and markers with a dark edge color are from F2 blades while the others are from the F1 blades. The trend line in black has a slope of 0.18 rad.

V. CONCLUDING REMARKS

We investigated experimentally the fluid structure problem of a two bladed flexible rotor in water. We show that at high Cauchy numbers the blades exhibit different behavior depending on the pitch angle : for high pitch the blades bend upstream and almost onto to the axis of rotation while for lower pitch they bend downstream. This discrepancy is rationalized using a geometrical argument measuring the local angle of attack at the blade tip. Regardless of the bending direction, the blades produce almost zero thrust at high Cauchy numbers. For moderate deformations up to 30 degrees of bending, the performance of the flexible blades is similar to the one of the rigid rotor. We found a strong link between the thrust produced and the blade deformation to the point where measuring the bending angle is sufficient to know the thrust.

Audoly, B. and Neukirch, S. (2021). A one-dimensional model for elastic ribbons: A little stretching makes a big difference. *Journal of the Mechanics and Physics of Solids*, 153:104457.

Cognet, V., Courrech du Pont, S., Dobrev, I., Massouh, F., and Thiria, B. (2017). Bioinspired turbine blades offer new perspectives for wind energy. *Proceedings of the Royal Society A: Mathematical, Physical and Engineering Sciences*, 473(2198):20160726.

Cognet, V., Courrech du Pont, S., and Thiria, B. (2020). Material optimization of flexible blades for wind turbines. *Renewable Energy*, 160:1373–1384.
de Langre, E. (2008). Effects of Wind on Plants. *Annual Review of Fluid Mechanics*, 40(1):141–168.
Durán Venegas, E., Le Dizès, S., and Eloy, C. (2019). A strongly-coupled model for flexible rotors. *Journal of Fluids and Structures*, 89:219–231.
Eldemerdash, A. and Leweke, T. (2021a). Fluid–structure interaction of a flexible rotor in water. *Journal of Fluids and Structures*, 103:103259.
Eldemerdash, A. S. and Leweke, T. (2021b). Deformation and wake of a flexible rotor in water. *Journal of Physics: Conference Series*, 1934(1):012006.
Glauert, H. (1983). *The Elements of Aerofoil and Airscrew Theory*. Cambridge University Press.
Gosselin, F., de Langre, E., and Machado-Almeida, B. A. (2010). Drag reduction of flexible plates by reconfiguration. *Journal of Fluid Mechanics*, 650:319–341.
Gosselin, F. P. and de Langre, E. (2011). Drag reduction by reconfiguration of a poroelastic system. *Journal of Fluids and Structures*, 27(7):1111–1123.
Hussain, M., Abdel-Nasser, Y., Banawan, A., and Ahmed, Y. M. (2021). Effect of hydrodynamic twisting moment on design and selection of flexible composite marine propellers. *Ocean Engineering*, 220:108399.
Li, H., Goodwill, T., Jane Wang, Z., and Ristroph, L. (2022). Centre of mass location, flight modes, stability and dynamic modelling of gliders. *Journal of Fluid Mechanics*, 937:A6.
Lissaman, P. B. S. (1983). Low-Reynolds-Number Airfoils. *Annual Review of Fluid Mechanics*, 15(1):223–239. _eprint: https://doi.org/10.1146/annurev.fl.15.010183.001255.
Lv, P., Prothin, S., Mohd-Zawawi, F., Benard, E., Morlier, J., and Moschetta, J.-M. (2015). Performance improvement of small-scale rotors by passive blade twist control. *Journal of Fluids and Structures*, 55:25–41.
Mateescu, D. and Abdo, M. (2010). Analysis of flows past airfoils at very low Reynolds numbers. *Proceedings of the Institution of Mechanical Engineers, Part G: Journal of Aerospace Engineering*, 224(7):757–775.
Motley, M., Liu, Z., and Young, Y. (2009). Utilizing fluid–structure interactions to improve energy efficiency of composite marine propellers in spatially varying wake. *Composite Structures*, 90(3):304–313.
Nguyen, D. Q., Loianno, G., and Ho, V. A. (2020). Towards Design of a Deformable Propeller for Drone Safety. In *2020 3rd IEEE International Conference on Soft Robotics (RoboSoft)*, pages 464–469, New Haven, CT, USA. IEEE.
Schouveiler, L. and Boudaoud, A. (2006). The rolling up of sheets in a steady flow. *Journal of Fluid Mechanics*, 563:71.
Sicard, J. and Sirohi, J. (2016). Aeroelastic stability of a flexible ribbon rotor blade. *Journal of Fluids and Structures*, 67:106–123.
Young, Y. (2008). Fluid–structure interaction analysis of flexible composite marine propellers. *Journal of Fluids and Structures*, 24(6):799–818.